Hindawi
Wireless Communications and Mobile Computing
Volume 2021, Article ID 8136833, 13 pages
https://doi.org/10.1155/2021/8136833

Research Article

A Study on the Diffraction Correction Prediction of Electromagnetic Field Intensity Based on the Method of Estimating Aerial Access Network Signal

Jialuan He,[1,2] Zirui Xing,[2] Qiang Wang,[2] Feihong Wu,[2] and Fuyong Lu[3]

[1]*School of Mechanical Electronic & Information Engineering, China University of Mining & Technology, Beijing 10083, China*
[2]*Beijing Aerocim Technology Co., Ltd., Beijing 102308, China*
[3]*Academy of China Open Economy Studies, University of International Business and Economics, Beijing 10029, China*

Correspondence should be addressed to Fuyong Lu; lufuyong@uibe.edu.cn

Received 13 June 2021; Accepted 19 August 2021; Published 13 September 2021

Academic Editor: Li-Xin Li

Field strength is a typical indicator of air access network signals, and the prediction of field strength has important reference significance for the estimation of aerial access network signals. However, many factors affecting the field strength, such as path, terrain, sunshine, and climate, increase the computational complexity, which greatly increases the difficulty of establishing an accurate prediction system. After persistent research by researchers in recent years, the ITU-R P.1546 model has gradually become a point-to-surface forecasting method for ground services recommended by ITU for ground operations in the frequency range of 30 MHz~3000 MHz. In view of the characteristics of electromagnetic signal propagation in mountainous environment, the influence of diffraction is also considered in this paper. Based on more accurate scene information such as actual terrain, the prediction calculation of electromagnetic signal propagation in a mountainous environment is proposed by using the corrected ITU-R P.1546 model. In addition, the influence of the actual terrain is taken into account to correct the relevant parameters, and the predicted results are compared with the measured data. The results indicate that field strength prediction results of the ITU-R P.1546 model based on the diffraction effect correction proposed in this paper in specific physical areas have better performance than those of the traditional ITU-R P.1546 model. Among them, the determination coefficient between the measured data and the predicted results is 0.87, the average error is 5.097 dBμV/m, and the root mean square error is 6.6228 dBμV/m, which proves that the ITU-R P.1546 model based on the corrected model is effective in the prediction of electromagnetic field intensity in the actual mountainous environment.

1. Introduction

As the air access network becomes more and more widely used, the signal estimation of the air access network becomes more and more important. Field strength is a typical indicator of aerial access network signals, so the prediction of field strength has important reference significance for the estimation of air access network signals. However, due to the numerous electromagnetic propagation scenarios, it is difficult to find a unified electromagnetic propagation model that can meet the requirements of all propagation modes, all frequency bands, all geographical environments, and all meteorological environments because of the numerous scenarios of electromagnetic propagation prediction and the variable requirements of prediction speed and accuracy. In general, the basic model should be selected according to the specific needs because of the different adaptations of various models to the terrain [1]. The similarities and differences of scenes are mainly reflected in the propagation path, such as ground-ground, ground-air, air-air, and earth-space [2, 3]. From the perspective of propagation mode, it is generally divided into several types, such as diffraction, scattering, direct radiation, refraction, and reflection, and the basic model calculates one or more combinations of them [4, 5]. From the perspective of frequency band, it can be generally divided into long wave, medium wave, short wave, ultrashort wave, microwave,

millimeter wave, etc. [6] The application range of the model can be limited to a single frequency band or across multiple frequency bands [7]. From the perspective of geographical environment, it is generally divided into low-lying hills, plains, mountainous areas, cold and warm fresh water, cold and warm seawater, forests, deserts, tundra, etc. [8, 9] The application scope of the models can be limited to a single geographical environment or simultaneously adapt to a variety of geographic environments [10].

As for the propagation prediction model of electromagnetic signals in the 30 MHz to 3000 MHz frequency band in the mountainous area and in the propagation path of ground-ground, the main basis has been the ITU-R P.370 mode in the past 50 years (1951-2001) [11, 12]. In addition, ITU-R P.1146 and ITU-R P.529 models were also applied to varying degrees on the corresponding period [13]. In the process of using ITU-R P.370, ITU-R P.1146, and ITU-R P.529 models, even if similar or even equal conditions are given, the prediction results also vary greatly [14].

In 2001, through the inheritance and integration of ITU-R P.370, ITU-R P.529, ITU-R P.1146, and other models, ITU-R Study Group 3 launched the ITU-R P.1546 model (the latest version is ITU-R P.1546-5 at present), which organically integrates ITU-R P.370, ITU-R P.529, ITU-R P.1146, and other models, forming a new forecast system [15, 16].

The ITU-R P.1546 propagation model is suitable for a point to area prediction, with the frequency range of 30 MHz to 3000 MHz, the distance range of 1-1000 km, the height of the transmitting antenna of lower than 3000 m, and the height of the receiving antenna of more than 1 m [17]. Compared with previous models, this model has been greatly improved in terms of simplification, scientificity, and maneuverability and can overcome the shortcomings of the original models in frequency and prediction distance [18, 19]. In the ITU-R P.1546 propagation model, the field strength is calculated by correcting based on table lookup. The correction terms include the following: mixed path correction, transmitting antenna height correction, transmitting antenna field intensity correction, clearance angle correction, receiving antenna correction, receiving end clearance angle correction, city short path correction, tropospheric scattering correction, time probability correction, frequency correction, and location probability correction [20–24].

In this paper, the ITU-R P.1546 model is firstly introduced, and then the field strength prediction method based on the ITU-R P.1546 model is described. For the coverage prediction of the high frequency band, the theoretical results of geometric optics and physical optics can be used for reference; diffraction effect correction is introduced. Finally, the ITU-R P.1546 model based on diffraction influence modification is used to predict the field intensity of the VHF radio station in the specific mountainous area, and the comparison and analysis are made with the measured data.

2. Materials and Methods

This section should contain sufficient detail so that all procedures can be repeated. It may be divided into headed subsections if several methods are described.

2.1. Overview of the ITU-R P.1546 Model. In the calculation of field intensity, the ITU-R P.1546 model has three main elements: transmitter antenna height, receiver antenna height, and clearance angle [25–27]. The value of the transmitting antenna height ht is related to terrain, propagation path, and sight distance. The effective height h_{ef} of the transmitting antenna in the land path is within 3~15 km (d) from the transmitting antenna to the receiving antenna path, which is higher than the average terrain height of the ground. The h_t of the sea surface path is the altitude of the antenna. Under the condition of land propagation path, the antenna height h_t and propagation horizon d must meet the following formula:

When the distance $d < 15$ km and there is no topographic data,

$$\begin{cases} h_t = h_e, \quad d \le 3, \\ h_t = \dfrac{h_e + (h_{ef} - h_e)(d-3)}{12}, \quad 3 \le d \le 15. \end{cases} \tag{1}$$

When the topographic data is known,

$$h_t = h_o. \tag{2}$$

When $d > 15$ km,

$$h_t = h_e, \tag{3}$$

where h_o is the antenna height above the average terrain height between $0.2d$and$d$(km) and h_e is the antenna height above the earth. When h_t is one of 10, 20, 37.5, 75, 150, 300, 600, and 1200 m, it can be calculated by

$$E = E_{\inf} + \frac{(E_{\sup} - E_{\inf}) \lg (h_t/h_{\inf})}{\lg (h_{\sup}/h_{\inf})} dB\left(\frac{uV}{m}\right), \tag{4}$$

where h_t is the height of the transmitter antenna and $h_{\inf}$ is the average height of the spread path. When the height of the receiving antenna is h_r (m), the reference field strength value is given by the land curve or table. When h_r is the lowest of 10 m, it corresponds to open areas such as suburbs. Height h_2 represents the covering height of the ground around the receiving antenna. When the actual receiving antenna h_2 is different from h_r, the correction terms related to the receiving environment need to be calculated. In order to facilitate the implementation of computer processing, the calculation method of correction term is further optimized and improved in the 1546 model, and the calculation flow chart is provided. For example, in the open area, the correction amount cor is expressed as

$$\begin{cases} \text{cor} = K_{h2} \lg \left(\dfrac{h_2}{h'}\right), \\ K_{h2} = 3.2 + 6.2 \lg (f), \end{cases} \tag{5}$$

where it is set as 10 m.

For the land path or mixed path environment, the correction value of the predicted field intensity can be obtained by terrain clearance angle, and then, the prediction accuracy can be improved. The clearance angle is the elevation angle from the receiving antenna to the direction of the transmitting antenna, which should be less than the height of the transmitting antenna, and the terrain is flat within the range of 0~16 km in its direction. The typical shading effect of the receiving point being slowly tilted by the terrain causes losses, which is fully taken into account in the land field intensity curve. Therefore, when θ_{tca} is a positive and small angle, additional correction compensation can not be considered. Based on the ITU-R P.370 model, the ITU-R P.1546 model only corrects part of the coefficients, including

$$\text{cor} = J\left(v'\right) - J(v). \tag{6}$$

In the formula,

$$\begin{aligned} J(v) &= \left[6.9 + 20\log\left(\sqrt{(v-0.1)^2+1} + v - 0.1\right)\right], \\ v' &= 0.036\sqrt{f}, \\ v &= 0.065\theta_{tca}\sqrt{f}. \end{aligned} \tag{7}$$

2.2. Diffraction Correction of Irregular Ground Obstacles. There may be one or several separate obstacles along the propagation path. In this scenario, the shape of the obstacle should be idealized, assuming it to be a blade with negligible thickness or a thick obstacle with smooth surface and ideal curvature at the top. The shape of the real obstacle is of course more complex, and some approximate treatment can be made for the basic obstacle here. Shorter propagation paths are studied in this section. When the path is too long to ignore the curvature of the earth, additional losses must be calculated. The following data apply to situations where the wave wavelength is much smaller than the size of the obstacle, i.e., in the VHF band or shorter wavelength ($f > 30$ MHz).

2.3. Single Edge Barrier. In a mountainous environment, there will be one or more separate obstacles on many propagation paths of electromagnetic signals. When calculating the field strength, the influence of obstacles in the propagation path on the signal propagation should be considered. In this paper, in diffraction correction, the case that there is a single obstacle in the direction of signal propagation is preliminarily considered and approximates to an ideal edge, and the edge model is used to correct the propagation of electromagnetic field intensity in mountainous areas.

According to the basic theoretical formula of diffraction, the signal field strength loss caused by a single edge obstacle is expressed as

$$J(v) = 6.9 + 20\log\left(\sqrt{(v-0.1)^2+1} + v - 0.1\right), \tag{8}$$

where v represents the basic parameter of the edge obstacle, which can be expressed as

$$v = h\sqrt{\frac{2}{\lambda}\left(\frac{1}{d_1} + \frac{1}{d_2}\right)}, \tag{9}$$

where λ represents the signal wavelength, d_1, d_2 represent the distance from the obstacle to the transmitter and receiver, respectively, and h represents the connecting part higher than the obstacle between the transmitter and receiver.

Ideally, all geometric parameters of an obstacle can be unified by a single dimensionless parameter:

$$v = h\sqrt{\frac{2}{\lambda}\left(\frac{1}{d_1} + \frac{1}{d_2}\right)}, \tag{10}$$

$$v = \theta\sqrt{\frac{2}{\lambda((1/d_1) + (1/d_2))}}, \tag{11}$$

$$v = \sqrt{\frac{2h\theta}{\lambda}}, \tag{12}$$

$$v = \sqrt{\frac{2d}{\lambda}\alpha_1\alpha_2}. \tag{13}$$

In the formula, h represents the part above the connecting line at the top of the obstacles at both ends of the connecting path. If it is below that line, then h is negative. d represents the path length, and d_1 and d_2 represent the distance from both ends of the path to the obstacle. The diffraction angle (radian) of α is the same plus-minus as that of h. α should be less than 0.2 radian, or 12°. α_1 and α_2 denote the angle between a line of vertex and path and the path connection. The symbols of α_1 and α_2 are the same as those of h. h, d, d_1, d_2found in Equations (10) to (13) should have a coordinated size with λ.

Loss (dB) is caused by the presence of obstacles in the function of v. When v is greater than -0.7, the approximation of the expression can be expressed as follows:

$$J(v) = 6.9 + 20\log\left(\sqrt{(v-0.1)^2+1} + v - 0.1\right). \tag{14}$$

2.4. Screen Barrier with Limited Thickness. Interference with a receiving station (or a small earth station) can also be imagined as an obstacle with a limited thickness across the propagation path, and its effect can be imagined as three edges, namely, the vertex and both ends of the obstacle. The interference caused by these three obstacles will cause rapid fading and fluctuation of the field strength at an integral multiple distance from the wavelength. In the following simplified model, the average and minimum diffraction loss estimation methods are given according to the location. Firstly, the minimum attenuation of a single edge is considered, and then, the average loss is obtained by comprehensive evaluation. This model comes from the consistent

diffraction theory (UTD) and has passed the high-precision measurement test.

(Step 1) The geometric parameters (vertex, left, and right ends) of each edge are calculated as formula (10) and (13).

(Step 2) Equation (14) is used to calculate the loss factor $j(v) = 10^{J(v)/20}$ of each edge.

(Step 3) The minimum diffraction loss $J_{\min}$ is calculated as follows:

$$J_{\min}(v) = -20 \log \left[\frac{1}{j_1(v)} + \frac{1}{j_2(v)} + \frac{1}{j_3(v)}\right]. \quad (15)$$

Or calculate the average value according to the following:

(Step 4) The following is the calculation of the average diffraction loss:

$$J_{\text{av}}(v) = -10 \log \left[\frac{1}{j_1^2(v)} + \frac{1}{j_2^2(v)} + \frac{1}{j_3^2(v)}\right]. \quad (16)$$

2.5. A Single Cylindrical Obstacle. Set the radius of the cylinder as R, note that the measured height at the highest point of the obstacle is h and the distance is d_1 and d_2, and then, the diffraction loss is

$$A = J(v) + T(m, n), \quad (17)$$

where $J(v)$ is the Fresnel-Kirchoff loss with the barrier vertex as the edge vertex. The dimensionless parameters can be calculated by Equations (10) to (13). For example, Equation (10) can be written as

$$v = 0.0316h\left[\frac{2(d_1 + d_2)}{\lambda d_1 d_2}\right]^{1/2}, \quad (18)$$

where h and v are in meters, and d_1 and d_2 are in kilometers. $J(v)$ is calculated by Equation (14). v is positive in the obstacles in the line-of-sight propagation, which can be calculated by Equation (14). $T(m, n)$ is the additional attenuation caused by the curvature of the obstacle:

$$T(m, n) = km^b, \quad (19)$$

where

$$\begin{aligned} k &= 8.2 + 12.0n, \\ b &= 0.73 + 0.27[1 - \exp(-1.43n)], \\ m &= R\frac{[(d_1 + d_2)/d_1 d_2]^{1/3}}{[\pi R/\lambda]}, \\ n &= h\frac{[\pi R/\lambda]^{2/3}}{R}. \end{aligned} \quad (20)$$

The dimensions of R, d_1, d_2, h, and k should be coordinated. $T(m, n)$ has the following properties: m and $T(m$ n) tend to 0 as R approaches 0. Therefore, in Equation (18), the cylinder with radius 0 is regarded as edge diffraction. Cylindrical models can be used extensively for ground modeling, but they are not applicable when there are paths across the water beyond the horizon, or very flat ground paths.

For two independent obstacles, the diffraction theory of a single edge can be used continuously to regard the top of the first obstacle as the source of the second obstacle. The geometric parameters of the first diffraction path are distances a and b and height h'_1, and its loss is L_1 (dB). The geometric parameters of the first diffraction path are distances b and c and height h'_2, and its loss is L_2 (dB). L_1 and L_2 are obtained by a fixed formula. The correction term L_c (dB) corresponds to the spacing b of the two edges. L_c is calculated as follows:

$$L_c = 10 \log \left[\frac{(a + b)(b + c)}{b(a + b + c)}\right]. \quad (21)$$

When both L_1 and L_2 are greater than 15 dB, the final loss is

$$L = L_1 + L_2 + L_c. \quad (22)$$

When the loss of two edges is similar, the above equation is more accurate. If a blade plays a major role, then, the geometric parameters of the first path are distances a and $b + c$ and height h_1, and the geometric parameters of the second path are distances b and c and height h'_2.

At this point, the single edge diffraction theory can be applied to two obstacles one by one. First, h/r is used to determine which is the main peak M, where h is the height of the apex of the edge and r is the radius of the first Fresnel ellipsoid, as shown in Equation (2). The loss of subpath MR is obtained by h'_2, and then, the T_c (dB) term is subtracted, that is, the part between two edges. The calculation of T_c (dB) is as follows:

$$T_c = \left[12 - 20 \log_{10}\left(\frac{2}{1 - (a/\pi)}\right)\right]\left(\frac{q}{p}\right)^{2p}, \quad (23)$$

where

$$\begin{aligned} p &= \left[\frac{2}{\lambda}\frac{(a + b + c)}{(b + c)a}\right]^{1/2} h_1, \\ q &= \left[\frac{2}{\lambda}\frac{(a + b + c)}{(a + b)c}\right]^{1/2} h_2, \\ &\tan\left[\frac{b(a + b + c)}{ac}\right]^{1/2}. \end{aligned} \quad (24)$$

The total loss is as follows:

$$L = L_1 + L_2 - T_c. \quad (25)$$

The same method is also applicable to other cylinders. When the obstacle is a flat top structure, it is not enough to simulate it with a single blade, and the phase sum of two parts needs to be calculated: one is the diffraction of the double edges, and the other is the reflection of the roof. When the reflection coefficient of the roof or the height difference between the roof and the side wall is not known, if the reflection part is ignored, the diffraction prediction value made by the double-edge model is very accurate.

2.6. General Approaches for One or More Obstacles. The following methods are applied to cases where there is one or more obstacles on the irregular path of line-of-sight propagation (including land and sea paths and line-of-sight or cross-horizon paths). The topographic profile of the radio propagation path is divided into a number of equidistant elevations, in which the elevations of the transmitter and receiver are the first and the last points, respectively, and the other points are some distance away from them. The height and distance of each point are recorded in the profile file.

In view of the different path profiles, the maximum parameter ν should be obtained first.

Each point between point a and point b ($a < b$) is recorded. When there is no intermediate point $a + 1 = b$, the diffraction loss of the path is 0. Otherwise, ν_n ($a < n < b$) is calculated one by one in order to select the maximum point of ν:

$$\nu_n = h\sqrt{\frac{2d_{ab}}{\lambda d_{\mathrm{an}} d_{nb}}}. \tag{26}$$

In the formula,

$$h = h_n + \left[\frac{d_{\mathrm{an}} d_{nb}}{2r_e}\right] - \left[\frac{(h_a d_{nb} + h_b d_{\mathrm{an}})}{d_{ab}}\right]. \tag{27}$$

D_{an}, d_{nb}, and d_{ab} are horizontal distances; h_a, h_b, and h_n are vertical heights; λ is wavelength; and r_e is effective earth radius. All h, d, r_e, and λ should be consistent.

The diffraction loss of the edge is obtained by Equation (14) when $J(\nu)$ is at $\nu > -0.78$; otherwise, the value is 0. Equation (26) is calculated directly from Equation (10). The second term of Equation (27), which represents a particular geometry, gives a good approximation of the curvature of the earth at the n^{th} point.

First, the above steps are used on the entire path from the transmitter to the receiver. The main edge is the point P with the maximum ν_p, and its loss is $J(\nu_p)$. The above steps are used twice at $\nu_p > -0.78$: ν_t and $J(\nu_t)$ are calculated from the transmitter to the main edge peak; ν_r and $J(\nu_r)$ are calculated from the main edge peak to the receiver. Other losses on this path are as follows:

$$\begin{gathered}\text{When } \nu_p > -0.78, L = J(\nu_p) + T[J(\nu_t) + J(\nu_r) + C], \\ \text{When } \nu_p < -0.78, L = 0,\end{gathered} \tag{28}$$

where C represents the empirical correction coefficient

$$C = 10.0 + 0.04D. \tag{29}$$

D represents the full length of the path (km), and

$$T = 1.0 - \exp\left[\frac{-J(\nu_p)}{6.0}\right]. \tag{30}$$

In the Deygout method, the path across the horizon includes at most 3 edges, among which, when the diffraction loss of the main peak is greater than 0, two secondary edges are still needed. When different effective earth radii are used for prediction on the same path profile, in order to avoid the problem of discontinuity caused by falling into the cycle of finding the point, the average effective earth radii of the main edge peaks and the auxiliary edge peaks on both sides can be obtained first, and then, the diffraction loss can be predicted with different effective earth radii.

2.7. Wedge-Shaped Obstruction with Finite Conduction. The following method is used to predict the diffraction loss of a wedge-shaped material with finite conduction, applicable to the diffraction loss caused by building angles and roof ridges or the wedge-shaped ridge topography. The requirement of this method is to obtain the conductivity and relative dielectric constant of the obstacle and to assume that there is no current transmission on the wedge surface. The method is based on the Unified Diffraction Theory (UTD), which also takes into account the diffraction of the shadow region and the line-of-sight region and the smooth transition of the predicted values between the two regions. The electric field value of the UTD formula at the field point is as follows:

$$e_{\mathrm{UTD}} = e_0 \frac{\exp(-jks_1)}{s_1} D^{\perp\!\!\!\parallel} \cdot \sqrt{\frac{s_1}{s_2(s_1 + s_2)}} \cdot \exp(-jks_2), \tag{31}$$

where e_0 represents the relative source amplitude, e_{UTD} represents the electric field value of the field point, k represents the number of waves, $2\pi/\lambda$, s_1 represents the distance between the source point and the diffraction edge, s_2 represents the distance between the field point of the diffraction edge, $D^{\parallel^{\perp}}$ represents the diffraction factor, depending on the incident angle of the diffraction edge (parallel or perpendicular to the incident axis), and the dimensions of s_1, s_2, and λ should be consistent. The diffraction factors of finitely

conducting wedges are as follows:

$$\begin{aligned} D^{\perp}_{\parallel} = {} & \frac{-\exp(-j\pi/4)}{2n\sqrt{2\pi k}} \left\{ \cot\left(\frac{\pi + (\Phi_2 - \Phi_1)}{2n}\right) \right. \\ & \cdot F\left(kLa^{+}(\Phi_2 - \Phi_1)\right) + \cot \\ & \cdot \left(\frac{\pi - (\Phi_2 - \Phi_1)}{2n}\right) \cdot F(kLa^{-}(\Phi_2 - \Phi_1)) \\ & + R_0^{\perp_{\parallel}} \cdot \cot\left(\frac{\pi - (\Phi_2 + \Phi_1)}{2n}\right) \\ & \cdot F(kLa^{-}(\Phi_2 + \Phi_1)) + R_n^{\perp_{\parallel}} \cdot \cot \\ & \cdot \left(\frac{\pi + (\Phi_2 + \Phi_1)}{2n}\right) \\ & \left. \cdot F\left(kLa^{+}(\Phi_2 + \Phi_1)\right)\right\}. \end{aligned} \tag{32}$$

In the formula, Φ_1 denotes the incident angle measured from the incident surface (0 surface), Φ_2 denotes the diffraction angle measured from the incident surface (0 surface), n denotes the external wedge angle, which needs to be multiplied by π (actual value $= n\pi$ (rad)), $j = \sqrt{-1}$, and $F(x)$ is the Fresnel integral:

$$F(x) = 2j\sqrt{x} \cdot \exp(jx) \cdot \int_{\sqrt{x}}^{\infty} \exp\left(-jt^2\right) dt, \tag{33}$$

$$\int_{\sqrt{x}}^{\infty} \exp\left(-jt^2\right) dt = \sqrt{\frac{\pi}{8}}(1-j) - \int_{0}^{\sqrt{x}} \exp\left(-jt^2\right) dt. \tag{34}$$

This integral can be computed by numerical integration. The above equation can be approximated as

$$\int_{\sqrt{x}}^{\infty} \exp\left(-jt^2\right) dt = \sqrt{\frac{\pi}{2} A(x)}, \tag{35}$$

where

$$A(x) = \begin{cases} \dfrac{1-j}{2} - \exp(-jx)\sqrt{\dfrac{x}{4}} \displaystyle\sum_{n=0}^{11} \left[(a_n + jb_n)\left(\frac{x}{4}\right)^n\right], & \text{if } x < 4 \\ -\exp(-jx)\sqrt{\dfrac{4}{x}} \displaystyle\sum_{n=0}^{11} \left[(c_n + jd_n)\left(\frac{4}{x}\right)^n\right], & \text{otherwise.} \end{cases} \tag{36}$$

$R_0^{\parallel^{\perp}}$, $R_n^{\parallel^{\perp}}$ are the reflection coefficients at vertical or parallel incidence:

$$\begin{aligned} R^{\perp} &= \frac{\sin(\Phi) - \sqrt{\eta - \cos(\Phi)^2}}{\sin(\Phi) + \sqrt{\eta - \cos(\Phi)^2}}, \\ R^{\parallel\parallel} &= \frac{b \cdot \sin(\Phi) - \sqrt{\eta - \cos(\Phi)^2}}{b \cdot \sin(\Phi) + \sqrt{\eta - \cos(\Phi)^2}}, \end{aligned} \tag{37}$$

where for R_0, $\Phi = \Phi_1$, for R_n, $\Phi = (n\pi - \Phi_2)$, $\eta = \varepsilon_r - j \times 10^9 \sigma/f$, ε_r represents the relative dielectric constant of wedge, σ represents the conductivity of wedge (S/m), and f represents frequency (Hz).

The two sides of the wedge may have different electric characteristics if necessary. At the boundary of shadow and reflection, the cotangent of Equation (32) becomes a singular value. $D^{\parallel^{\perp}}$ is an estimable finite value. For small finite values, the term containing the singular tangent function becomes

$$\begin{aligned} & \cot\left(\frac{\pi \pm \beta}{2n}\right) \cdot F\left(kLa^{\pm}(\beta)\right) \cong n \cdot \left[\sqrt{2\pi kL} \cdot \operatorname{sign}(\varepsilon) - 2kL\varepsilon \cdot \exp\left(\frac{j\pi}{4}\right)\right] \\ & \cdot \exp\left(\frac{j\pi}{4}\right). \end{aligned} \tag{38}$$

ε is defined as

$$\begin{aligned} &\text{When } \beta = \Phi_2 + \Phi_1, \varepsilon = \pi + \beta - 2\pi n N^{+}, \\ &\text{When } \beta = \Phi_2 - \Phi_1, \varepsilon = \pi - \beta + 2\pi n N^{-}. \end{aligned} \tag{39}$$

This makes the diffraction factor continuous at the boundary of the shadow and reflection region, since the same reflection coefficients are used to calculate the reflection rays. The electric field e_{LD} of the domain is as follows when $(\Phi_2 - \Phi_1) < \pi$:

$$e_{\mathrm{LD}} = \begin{cases} e_{\mathrm{UTD}} + \dfrac{\exp(-jks)}{s}, & \text{when } \Phi_2 < \Phi_1 + \pi, \\ e_{\mathrm{UTD}}, & \text{when } \Phi_2 \geq \Phi_1 + \pi. \end{cases} \tag{40}$$

In the formula, s represents the straight-line distance between the source and the domain point. When $(\Phi_2 - \Phi_1) < \pi$, the second cotangent term of Equation (34) becomes a singular value, which should be approximated by Equation (38). The field strength ratio (dB) of wedge-shaped obstacle and non-wedge-shaped obstacle can be expressed as the decibel value relative to the free space. At this time, e_0 in Formula (31) can be normalized, and its calculation is as follows:

$$E_{\mathrm{UTD}} = 20 \log\left(\left|\frac{s \cdot e_{\mathrm{UTD}}}{\exp(-jks)}\right|\right). \tag{41}$$

In the formula, s represents the straight-line distance between the source and the domain point. When $n = 2$ and

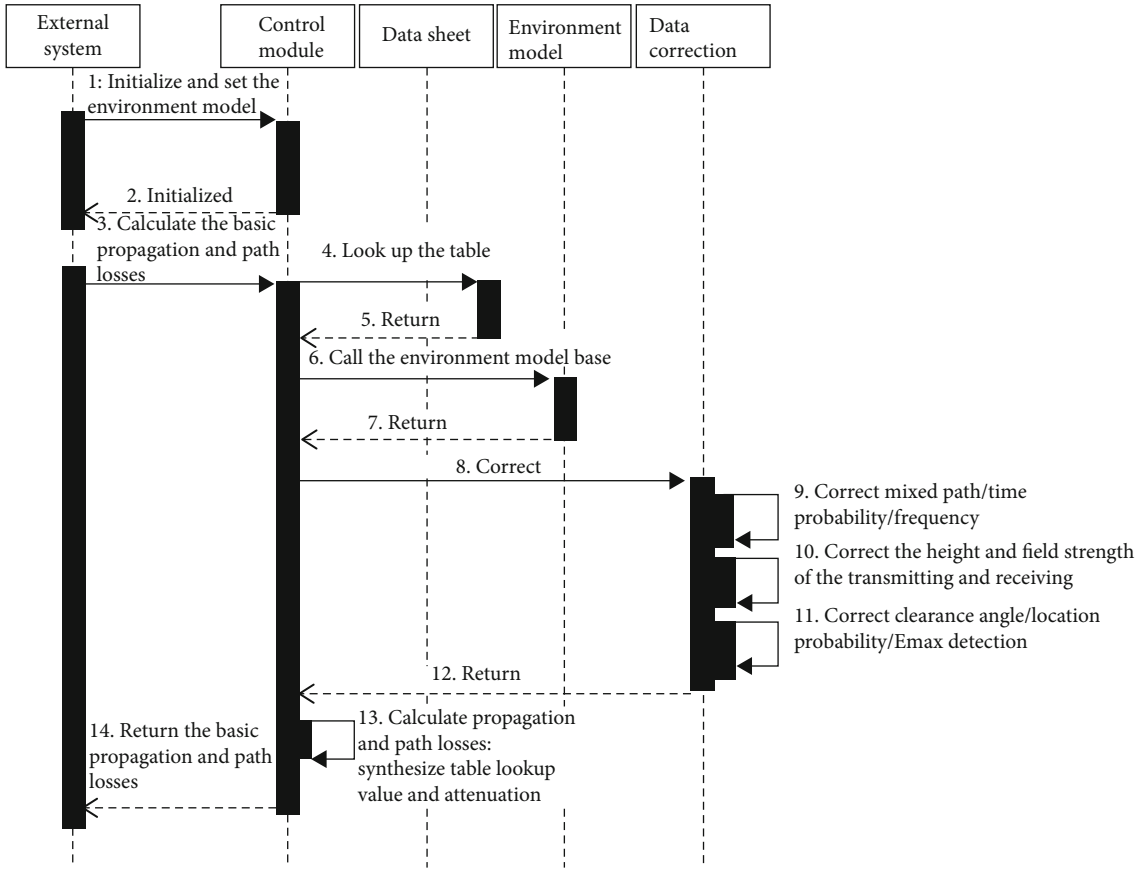

Figure 1: Basic processing flow of propagation model.

the reflection coefficient is 0, the result of this formula is the same as that of the edge diffraction.

2.8. Correction Steps of Electromagnetic Field Intensity Prediction Diffraction. The following method is used to predict the diffraction loss of a wedge-shaped material with finite.

In accordance with the basic processing flow of the electromagnetic signal propagation model as shown in Figure 1, the main steps of predicting the field intensity distribution with the 1546 model include:

(Step 1) Initialize and set the environment model.

(Step 2) Initialize and return parameter state.

(Step 3) Calculate the basic propagation and path losses.

(Step 4) Look up the table.

(Step 5) Return the table lookup value.

(Step 6) Call the environment model base.

(Step 7) Return environmental data.

(Step 8) Correct.

(Step 9) Correct mixed path/time probability/frequency.

(Step 10) Correct the height and field strength of the transmitting and receiving antennas.

(Step 11) Correct clearance angle/location probability/Emax detection.

(Step 12) Return the corrected value.

(Step 13) Calculate propagation and path losses: synthesize table lookup value and attenuation value.

(Step 14) Return the basic propagation and path losses.

3. Results and Discussion

3.1. Subheadings. In order to verify and evaluate the performance of the electromagnetic field strength prediction method based on the ITU-R P.1546 model, a method is designed in this paper to evaluate the performance of the method in the field strength prediction by comparing the simulation prediction with the measured data. The 1546 model, which does not take the diffraction effect correction into account, is also calculated and compared in the simulation prediction. The main difficulty of the simulation prediction is how to extract the corresponding parameters based on more detailed terrain, ground objects, and other data to correct the propagation model. However, the difficulty of the measured data acquisition lies in the uncontrollable factors in the electromagnetic environment, among which the

Table 1: List of predicted and measured field strength.

Longitude	Latitude	Height	Measured field strength	Modified model Prediction results	Uncorrected modified model Prediction results	ICS software Prediction results
117.47044	36.42849	495	22.784	28.0166	18.2799	18.5234
117.47044	36.428488	495	38.7592	43.0306	18.28	18.7358
117.47013	36.427628	495	25.8452	26.4031	18.5257	16.1948
117.47012	36.427626	495	36.0796	36.7268	18.5258	20.2752
117.46981	36.426766	495	31.3682	28.5766	18.5927	17.5079
117.46981	36.426763	495	19.3239	19.754	18.5928	19.0938
117.4695	36.425903	495	25.0864	30.373	18.6013	17.1426
117.4695	36.425901	495	35.7749	36.082	18.6014	20.2773
117.46919	36.425041	414	33.4743	32.122	18.6591	18.8263
117.46919	36.425038	414	35.6233	36.3091	18.6593	19.7894
117.46888	36.424178	414	26.7722	32.428	18.6676	20.3606
117.46888	36.424176	414	35.708	39.1348	18.6677	17.2056
117.46856	36.423316	414	28.7753	31.3567	18.7319	19.846
117.46856	36.423313	414	34.6269	37.1839	18.732	18.1015
117.46825	36.422453	414	33.7977	32.8018	18.7933	18.7942
117.46825	36.422451	414	35.6533	37.9868	18.7934	18.0807
117.46794	36.421591	414	33.5383	34.6322	18.8039	20.0508
117.46794	36.421589	414	26.8122	31.555	18.804	20.563
117.46763	36.420729	414	23.6421	28.0866	18.8621	17.7462
117.46763	36.420726	414	39.1774	39.783	18.8623	20.0933
117.46731	36.419866	414	61.04	38.9964	18.8726	18.4299
117.46731	36.419864	414	69.04	39.6481	18.8728	18.3112
117.467	36.419002	414	62.04	26.7161	18.9524	20.5299
117.467	36.419	414	57.04	22.6321	18.9526	17.7656
117.46723	36.418124	314	68.04	37.9287	19.0185	20.2808
117.46723	36.418121	314	72.04	40.2566	19.0187	20.9546
117.46747	36.417246	314	60.04	35.0796	19.0667	20.7386
117.46747	36.417243	314	64.04	25.0355	19.0669	16.0675
117.4677	36.416367	314	96.04	37.1593	19.1332	19.3316
117.4677	36.416364	314	69.04	23.4415	19.1334	17.496
117.46793	36.415489	314	56.04	39.5785	19.1998	19.8891

most important ones are the uncontrollable external disturbance and self-disturbance.

In this paper, the determination coefficient, root mean square error, and average error are used to measure the accuracy, as follows.

$$R^2\left(E_{\text{pre}}, E_{\text{rea}}\right) = \frac{\text{COV}^2\left(E_{\text{pre}}, E_{\text{rea}}\right)}{\text{Var}\left(E_{\text{pre}}\right) Var\left(E_{\text{rea}}\right)}. \tag{42}$$

In the formula, E_{pre} is the predicted result of field intensity output by the model, and E_{rea} is the measured result of field intensity.

$$\sigma_E = \sqrt{\frac{1}{N}\sum_{i=1}^{N}\left(E_{\text{pre},i} - E_{\text{rea},i}\right)}. \tag{43}$$

In the formula, σ_E is the root mean square error of the predicted field strength relative to the measured value.

$$\text{err} = \frac{1}{N}\sum_{i=1}^{N}\left|E_{\text{pre},i} - E_{\text{rea},i}\right|. \tag{44}$$

err is the mean absolute error between the predicted and measured field strength values.

The field intensity observation experiment was conducted in two different mountainous areas by means of ultrashort wave radio, matching antenna, and power supply equipment. In addition, a mobile vehicle equipped with receiving antenna and other related equipment was used to collect and measure the field intensity corresponding to the electromagnetic signals at multiple points. Combined with the physical geography of the mountains and the basic parameters of experimental equipment, the field intensity

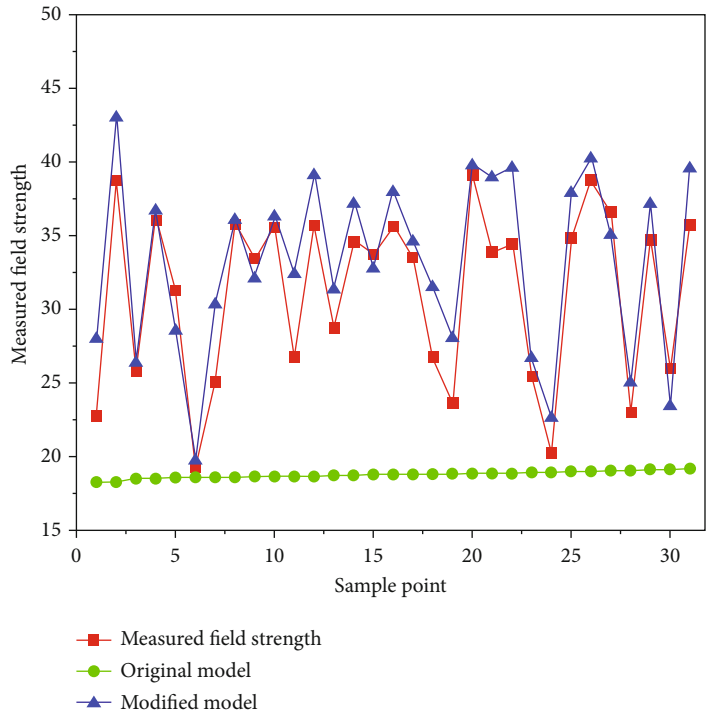

(a)

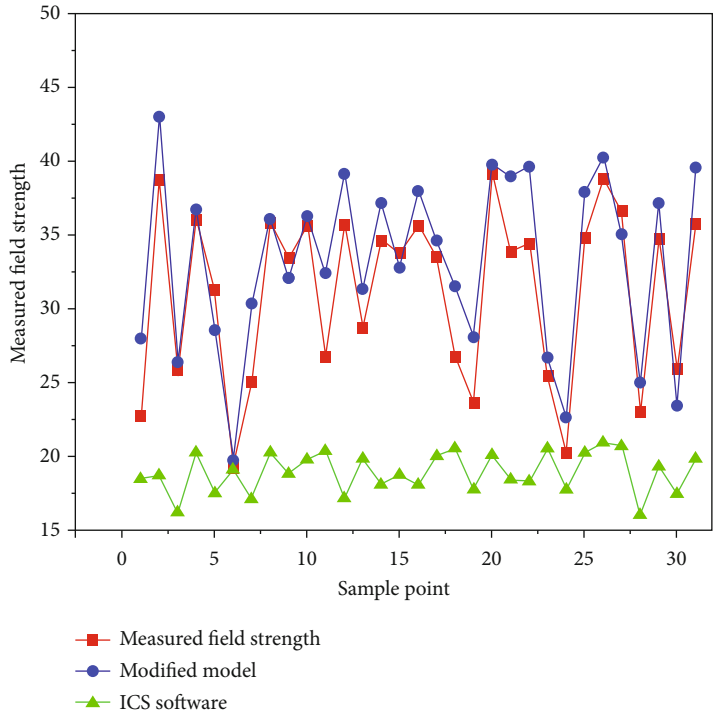

(b)

Figure 2: (a) Predicted field strength by the original model and the modified model in area A. (b) Predicted field strength and measured field strength distribution in area A.

distribution of ultrashort wave radio in this region was simulated and calculated.

3.2. Results in Area A. The modified model, original model, and ICS software are used in area A to predict the field strength and compared with the actual measured value. The typical measurement results in areas with large height fluctuations are shown in Table 1. The comparison between the original model and the modified model is shown in Figure 2(a), and the comparison between the

Table 2: List of predicted and measured field strength.

Longitude	Latitude	Height	Measured field strength	Modified model Prediction results	Uncorrected modified Model prediction results	ICS software Prediction results
117.708	35.85517	178	46.2366	45.8832	29.5598	30.8491
117.708	35.85517	178	47.098	46.75	29.5596	28.1712
117.7085	35.85437	178	43.7944	42.7128	29.4799	29.3088
117.7085	35.85437	178	48.1022	52.1082	29.4797	29.6885
117.709	35.85357	178	45.3714	46.9492	29.3958	30.1577
117.709	35.85357	178	43.8045	46.0795	29.3956	28.5521
117.7095	35.85277	178	47.5033	51.2638	29.3158	31.2398
117.7095	35.85276	178	36.5418	38.1916	29.3156	27.1532
117.71	35.85196	185	39.4194	45.1655	29.2375	26.6682
117.71	35.85196	185	34.8515	34.2715	29.2373	26.866
117.71	35.8519	185	38.4794	40.3106	29.2312	29.6204
117.71	35.8519	185	32.3551	33.0539	29.2312	29.2735
117.7108	35.85126	185	43.3582	44.7876	29.1548	27.1326
117.7108	35.85126	185	35.8553	37.4266	29.1548	29.4299
117.7116	35.85062	185	43.8938	48.3461	29.0734	27.6986
117.7116	35.85062	185	30.7923	29.8799	29.0733	26.498
117.7123	35.84998	179	29.239	33.4362	18.2181	15.3102
117.7123	35.84998	179	28.8912	26.3211	18.2181	16.6991
117.7131	35.84935	179	38.5259	38.369	23.8795	25.4416
117.7131	35.84934	179	41.3282	46.9653	23.8794	23.8747
117.7139	35.84871	179	39.436	43.0395	28.8348	28.6936
117.7139	35.84871	179	46.3841	44.1824	28.8347	26.9046
117.7147	35.84807	179	33.2248	33.6186	28.7607	28.1243
117.7147	35.84807	179	40.3965	42.7377	28.7607	26.6967
117.7155	35.84743	179	49.6388	47.1077	28.6856	29.1129
117.7155	35.84743	179	48.7131	50.1768	28.6855	26.2339
117.7162	35.84679	179	42.3141	43.5969	28.5897	27.1897
117.7162	35.84679	179	48.9966	47.8809	28.5896	28.7789
117.717	35.84615	179	36.9246	40.7389	28.4993	26.0008
117.717	35.84615	179	46.9615	45.2969	28.4992	30.259
117.7178	35.84551	179	41.72	43.0521	28.4169	29.1489
117.7178	35.84551	179	40.0697	44.1006	28.4168	27.5862
117.7186	35.84487	186	36.3089	34.9426	28.3361	28.1167
117.7186	35.84487	186	46.1627	43.2275	28.336	28.318

modified model and the ICS software is shown in Figure 2(b).

As shown in Table 1, the height of this sampled data group fluctuates greatly, and the height fluctuates nearly 200 meters. It can be clearly seen from Figure 2(a) that compared with the original ITU-R P.1546 model, the field strength prediction results based on the revised ITU-R P.1546 model are in good agreement with the measured field strength data. According to formulas (42) and (44), the determination coefficient of the modified model is 0.845, the root mean square error is 5.931 dBμV/m, and the average absolute error is 2.603 dBμV/m, while the determination coefficient of the original model is 0.006.

It can be seen from Figure 2(b) that compared with the calculation results of the ICS software, the field strength prediction results based on the revised ITU-R P.1546 model are closer to the actual measured results in terms of value and trend. The determination coefficient of the results of the ICS software is 0.169, so it can be seen from the statistical analysis results that the modified model has a much higher coefficient of determination, indicating that compared with the original model and ICS software, the modified ITU-R P.1546 model can adapt to this mountainous area with obvious topography.

What is more, a total of 3884 sets of data tested in mountain area A are statistically analyzed. The determination coefficient of the modified model is 0.976, the root mean square error is 16.927 dBμV/m, and the average absolute error is 2.527 dBμV/m.

According to the discussion above, compared with the original model and ICS software, the modified ITU-R

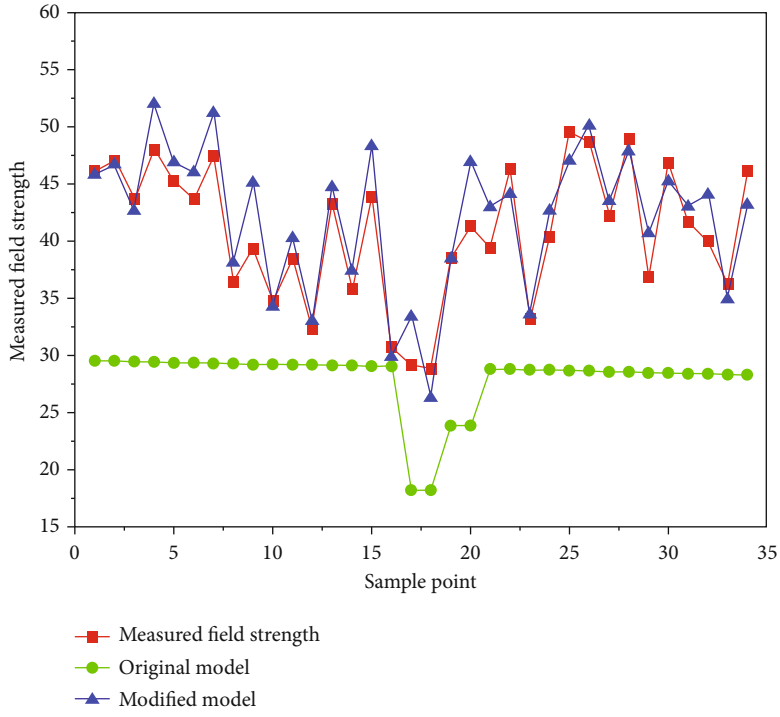

(a)

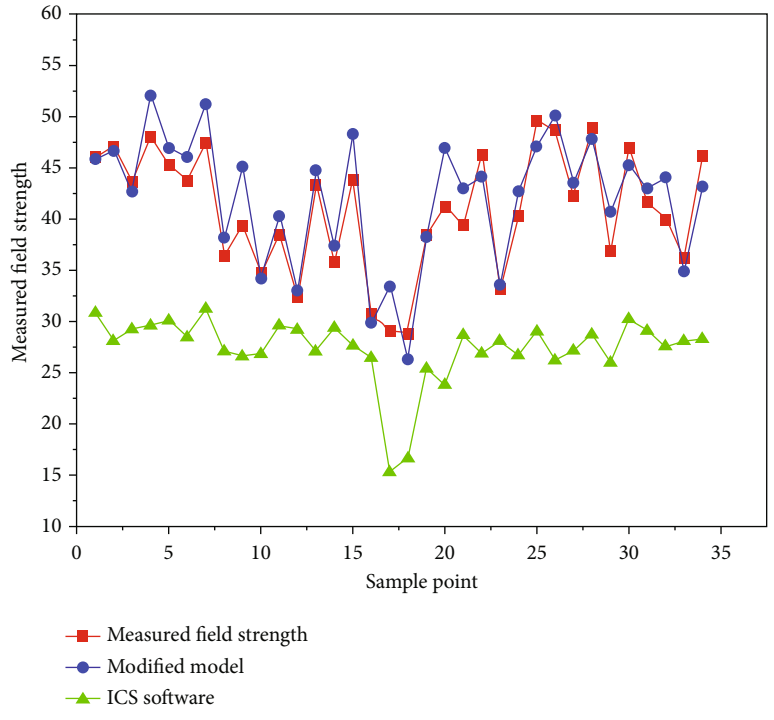

(b)

Figure 3: (a) Predicted field strength by the original model and the modified model in area B. (b) Predicted field strength and measured field strength distribution in area B.

P.1546 model is very relevant in mountain area A with obvious undulations, which can adapt to the mountain area, improve the prediction accuracy, and make better predictions.

3.3. Results in Area B. The same test was carried out in area B. The typical results in areas with less height fluctuations are shown in Table 2. The comparison between the original model and the revised model is shown in Figure 3(a), and

the comparison between the revised model and the ICS software is shown in Figure 3(b).

As shown in Table 2, it can be seen that the height fluctuation of this sampling data group is small and the maximum height difference is only 8 meters. It can be clearly seen from Figure 3(a) that compared with the original ITU-R P.1546 model, the field strength prediction results based on the revised ITU-R P.1546 model have a high consistency with the measured field strength data. The statistical analysis shows that the determination coefficient of the modified model is 0.848, the root mean square error is 6.026 dBμV/m, and the average absolute error is 2.203 dBμV/m.

Compared with Figure 2(b), it can be seen from Figure 3(b) that in this region with small height fluctuations, the field strength prediction of the ICS software has similar trends to the actual measured results, but there is still a big gap between the prediction and the actual results. The field strength prediction results based on the revised ITU-R P.1546 model are closer to the actual measurement results in terms of trends and values.

What's more, a total of 3980 sets of test data in mountain area B are statistically analyzed. The determination coefficient of the modified model is 0.978, the root mean square error is 15.365 dBμV/m, and the average absolute error is 1.992 dBμV/m.

According to the discussion above, in areas with relatively mild fluctuations, the trends of various prediction methods are closer to the actual measured values, but the prediction results of the modified model are still significantly better than those of other prediction methods, indicating that the modified ITU-R P.1546 model is better than other models and can predict the field strength distribution in mountainous areas better.

4. Conclusions

Electromagnetic propagation simulation is the basis of various electromagnetic equipment simulation and electromagnetic analysis and calculation, which directly determines the fidelity, timeliness, and usability of various simulation calculations. In this paper, the ITU-R P.1546 model, launched by ITU, is introduced to calculate the propagation distribution of electromagnetic waves under complex terrain and complex meteorological conditions. In this paper, the model algorithm and the calculation process of electromagnetic signal field intensity were firstly analyzed, and the verification experiment was conducted in the mountainous environment. On the basis of more accurate scene information such as actual terrain and taking into account the influencing factors such as actual terrain to correct the relevant parameters in the model, the test results in the mountainous areas of A and B prove that the method of modifying the ITU-R P.1546 model for field strength prediction by considering the diffraction factors in the mountainous environment is effective and further improves the traditional ITU-R P.1546 model's field strength prediction accuracy.

The focus of this paper is only on the case of a single obstacle, but there are many peaks in the actual mountain environment. Therefore, in a future work, it is necessary to give full consideration to how to further improve the field strength prediction algorithm based on the ITU-R P.1546 model under the condition of approximately random distribution of obstacles.

Data Availability

The (area A and area B) data used to support the findings of this study were supplied by Jialuan He under license and so cannot be made freely available. Requests for access to these data should be made to Jialuan He, Beijing Aerospace Chenxin Technology Co., Ltd., Beijing, 102308, China (hejialuan@163.com).

Conflicts of Interest

There is no conflict of interest regarding the publication of this paper.

Acknowledgments

This work was supported in part by Clinical Medicine Plus X-Young Scholars Project, Peking University, the Fundamental Research Funds for the Central Universities (BMU2021PYB034), and the National Natural Science Foundation Project (51674269).

References

[1] E. Ostlin, H. M. Zepernick, and H. Suzuki, "Evaluation of the new semi-terrain based propagation model recommendation ITU-R P.1546," in *2003 IEEE 58th Vehicular Technology Conference. VTC 2003-Fall (IEEE Cat. No.03CH37484)*, Orlando, FL, USA, 2003.

[2] M. Mayrink, F. Moreira, C. G. Rego, M. Burian, and E. V. Melo, "Improving the treatment of mixed-terrain paths of the recommendation ITU-R P.1546 for the path-loss prediction of short UHF links," in *SBMO/IEEE MTT-S International Conference on Microwave and Optoelectronics, 2005*, Brasilia, Brazil, 2005.

[3] F. Song, Z. Ai, Y. Zhou, I. You, K. R. Choo, and H. Zhang, "Smart collaborative automation for receive buffer control in multipath industrial networks," *IEEE Transactions on Industrial Informatics*, vol. 16, no. 2, pp. 1385–1394, 2020.

[4] L. Paunovska and L. Gavrilovska, "Comparison of propagation models ITU.R-P.1546 and ITU.R-P.1812," in *2014 4th International Conference on Wireless Communications, Vehicular Technology, Information Theory and Aerospace & Electronic Systems (VITAE)*, Aalborg, Denmark, 2014.

[5] R. F. Liao, H. Wen, J. Wu, H. Song, F. Pan, and L. Dong, "The Rayleigh fading channel prediction via deep learning," *Wireless Communications and Mobile Computing*, vol. 2018, Article ID 6497340, 11 pages, 2018.

[6] Y. Okumara, E. Ohmori, T. Kawano, and K. Fukuda, *Field strength variability in VHF and UHF land mobile service*, Review of the Electrical Communication Laboratory, 1968.

[7] C. Yang, J. Wang, X. You, S. U. Haibin, J. I. Shengyu, and Z. Zhao, "Applicability of ITU-R P.1546 recommendation in

typical terrestrial areas of CHINA," *Chinese Journal of Radio Science*, 2019.

[8] J. Jorge, M. Oswaldo, J. Ramírez, and M. Víctor, "Potential use of IEEE 802.11af standard in the radioeletric spectrum for VHF and UHF bands in urban areas," in *IV Congreso Internacional de Ciencia, Tecnología e Innovación Para la Sociedad*, 2017.

[9] F. Song, Z. Ai, H. Zhang, I. You, and S. Li, "Smart collaborative balancing for dependable network components in cyber-physical systems," *IEEE Transactions on Industrial Informatics*, vol. 17, no. 10, pp. 6916–6924, 2021.

[10] I. Joo and C. Sin, "Design of GNSS jamming propagation simulator using ITU-R P.1546 propagation model," in *2015 15th International Conference on Control, Automation and Systems (ICCAS)*, pp. 1359–1362, Busan, Korea (South), 2015.

[11] B. Itur, *P.370-7, VHF and UHF propagation curves for frequency range from 30 MHz to 1000 MHz*, International Telecommunication Union, 1995.

[12] F. Song, Y. T. Zhou, Y. Wang, T. Zhao, I. You, and H. K. Zhang, "Smart collaborative distribution for privacy enhancement in moving target defense," *Information Sciences*, vol. 479, pp. 593–606, 2019.

[13] K. Allsebrook and J. D. Parsons, "Mobile radio propagation in British cities at frequencies in the VHF and UHF bands," *IEEE Transactions on Vehicular Technology*, vol. 26, no. 4, pp. 313–323, 2013.

[14] W. P. Liu, B. Cao, Z. G. Liu, K. Liu, and Z. H. Tang, *Simulation Analysis to Influence of Irregular Topography on ADS-B Ground Station Signal Coverage*, Electronics Optics & Control, 2016.

[15] I. Stevanovic, "MATLAB/Octave Implementation of Recommendation ITU-R P.1546 "Method for Point-to-Area Predictions for Terrestrial Services in the Frequency Range 30 MHz to 4 000 MHz"," *Computer Science and Engineering*, 2021.

[16] J. Kalliovaara, R. Ekman, T. Jokela, M. Jakobsson, and M. Meriläinen, "Suitability of ITU-R P.1546 propagation predictions for allocating LTE SDL with GE06," in *The IEEE International Symposium on Broadband Multimedia Systems and Broadcasting 2017*, Cagliari, Italy, 2017.

[17] S. Kasampalis, P. I. Lazaridis, Z. D. Zaharis, A. Bizopoulos, S. Zettas, and J. Cosmas, "Comparison of Longley-Rice, ITU-R P.1546 and Hata-Davidson propagation models for DVB-T coverage prediction," *Scientometrics*, vol. 21, no. 1, pp. 99–113, 2014.

[18] H. Suzuki and H. J. Zepernick, "Evaluation of the propagation model recommendation ITU-R P.1546 for mobile services in rural Australia," *IEEE Transactions on Vehicular Technology*, vol. 57, no. 1, pp. 38–51, 2008.

[19] F. Song, M. Zhu, Y. Zhou, I. You, and H. Zhang, "Smart collaborative tracking for ubiquitous power IoT in edge-cloud interplay domain," *IEEE Internet of Things Journal*, vol. 7, no. 7, pp. 6046–6055, 2020.

[20] S. Popov, J. Günther, H. P. Seidel, and P. Slusallek, *Stackless KD-Tree Traversal for High Performance GPU Ray Tracing*, John Wiley & Sons, Ltd., 2010.

[21] G. Koudouridis and P. Soldati, *Trading Off Network Density with Frequency Spectrum for Resource Optimization in 5G Ultra-Dense Networks*, Technologies, 2018.

[22] S. Popov, "Stackless KD-tree traversal for high performance GPU ray tracing," *Computer Graphics Forum*, vol. 26, no. 3, pp. 415–424, 2007.

[23] L. A. Akinyemi, O. Shoewu, O. A. Pinponsu, J. O. Emagbetere, and F. O. Edeko, "Effects of base transceiver station (BTS) on humans in Ikeja area of Lagos State," *Pacific Journal of Science and Technology*, vol. 3, no. 8, pp. 28–34, 2014.

[24] T. Schmidt-Dumont and J. H. Van Vuuren, "Optimisation of radio transmitter locations in mobile telecommunication networks," *South African Journal of Industrial Engineering*, vol. 27, no. 2, pp. 160–176, 2016.

[25] International Telecommunication Union, *Method for Point-to-Area Predictions for Terrestrial Services in the Frequency Range 30 MHz to 4 000 MHz*, Electronic Publication, 2019.

[26] ITU-R, *Method for Point-to-Area Predictions for Terrestrial Services in the Frequency Range 30 MHz to 3000 MHz*, Recommendation ITU-R P, 2003.

[27] K. Paran and N. Noori, "Tuning of the propagation model ITU-r p.1546 recommendation," *Progress in Electromagnetics Research B*, vol. 8, pp. 243–255, 2008.